J. Ind. Geophys. Union, 30(2) (2026), 102-113
https://doi.org/10.71122/JIGU.30(2)2026.0011

Laser Raman characterization and 3D mapping of chromite crystal from Asurabandha mines of Bhuban ultramafic complex, Odisha (India)

Ashish Gupta and Dinesh Pandit*
Department of Geology, Institute of Science, Banaras Hindu University, Varanasi - 221005, India,
Corresponding author: dpandit@hotmail.com

ABSTRACT

The Asurabandha chromite deposits are hosted in the Bhuban Ultramafic Complex (BUC), which is located in the Dhenkanal district of Odisha. The BUC forms part of the transition domain between the Singhbhum Craton and the Eastern Ghats Mobile Belt (EGMB). Highly altered chromitite rocks are found as isolated, irregular and sporadic orebodies located on the southern side of the Sukinda Ultramafic Complex (SUC) accompanied by the granite-charnockite association. Petrographic studies inferred the existence of heteradcumulate texture in the chromitite rock, which indicates early crystallization during the cooling of an ultramafic magma. Chromite begins to crystallize at a high temperature and accumulates to growth of crystal framework, subsequently crystallizing to form silicate minerals (olivine or pyroxene), that later altered to serpentine. Occurrences of euhedral chromite crystal indicates inherent crystal growth during the crystallization of magma. The Laser Raman Micro Spectroscopy (LRMS) analysis, displays four characteristics Raman Shift at 454, 559, 736 and 1437 cm^{-1} for chromite and five diagnostic Raman Shift at 127, 206, 397, 465 and 1166 cm^{-1} for serpentine. Laser Raman-SNOM scanning, 2D and 3D mapping of euhedral hexagonal chromite crystal, suggests its heterogenous internal crystal structure in the ultramafic rocks. In the chromite crystal, internal heterogeneity may appear because of trace element substitution during the magmatic crystallization or secondary alteration processes like serpentinization and carbonation. The Asurabandha chromite deposits are characterized by metasomatic alteration, serpentinization and carbonation, where original silicate minerals have been replaced by serpentine, presenting challenges for mineral exploration due to the extent beyond lateritic overburden.

Keywords: Laser Raman, Chromite, Serpentine, Ultramafic Rocks, Asurabandha, Bhuban Ultramafic Complex, Singhbhum craton.

INTRODUCTION

The Laser Raman Micro Spectroscopy (LRMS) is an in-situ scientific technique that uses inelastic scattering of light from a laser to provide a chemical 'fingerprint' of a sample's vibrational, rotational, and other low-frequency vibrational modes (Raman, 1922; Hope et al., 2001). By measuring the Raman Shift (the difference in frequency between the scattered and incident light), one can identify molecules, analyse their structure, and determine their composition in various forms, including solids, liquids, and gases (Raman, 1923). The technique requires a laser beam for excitation, a sample interface, and a spectrometer to disperse and detect the scattered light (Raman, 1942, 1947). The LRMS technique is applied to identify minerals by analysing light scattering, which creates a unique "spectral fingerprint" from a mineral's atomic vibrations (McMillan, 1989; Keresztury, 2006). This non-destructive method requires little to minimum sample preparation, complementing other techniques like Scanning Electron Microscopy (SEM) and X-ray Diffraction (XRD) to provide detailed chemical and structural information. This Laser Raman technique is valuable for fieldwork and identifying difficult-to-discern minerals like light-coloured silicates. A mineral sample is exposed to a monochromatic light beam, usually a laser. The light interacts with the mineral's chemical bonds, causing some of the light to scatter inelastically (Raman, 1927, 1928; Raman and Krishnan, 1928). The scattered light has a unique energy shift or Raman Shift depending on the mineral's crystal structure, atomic masses, bond-lengths, and bond-angles (Raman, 1929, 1945). A spectrometer captures this scattered light and analyses the energy shifts to produce a unique spectrum or Raman Shift or "fingerprint," for that mineral.

The LRMS's ability to provide rapid identification of mineral phases is beneficial for exploration, especially for minerals that are hard to identify optically using a polarising microscope (Rodgers, 1993; Bersani and Lottici, 2016). This method helps to differentiate between minerals with similar appearance but different chemical compositions, such as various silicate, sulphide and carbonate groups (Pandit, 2024). It is also useful for identifying opaque or weathered grains that are difficult to analyse with traditional optical microscopy (Singh and Pandit, 2025). This is a non-destructive technique and does not alter or destroy the sample. Minimal sample preparation is required for the LRMS studies, which means samples often require no specific preparation. It can be used on a wide variety of sample types and sizes, from small powders to large piece of samples. The LRMS is a valuable tool when simultaneously used with microscopy and X-ray diffraction to identify minerals.

The objective of this study is emphases on phase recognition in the mineralized ultramafic rocks by analysing a mineral's physical and optical properties, crystalline structure, size, shape, and textural position to identify their petrogenetic implications. The characterization of mineral phases in the ultramafic rock involving the LRMS technique with the help of 532 nm wavelength excitation. In general, the essential minerals found in ultramafic rocks are olivine and pyroxene, with smaller amounts of garnet and spinel. Chromite is an important economic mineral found predominantly in ultramafic rocks, which include peridotite, dunite, and serpentinite.

Characterization of mineral phases in ultramafic rocks will help to understand the origin of chromite crystals in the orebody of the Asurabandha deposits, located in the Dhenkanal district of Odisha.

REGIONAL GEOLOGY

The Singhbhum Craton is an ancient geological terrain in the Jharkhand and Odisha states of India, characterized by its >3.5 Ga old Archean granite and greenstone belts. The Singhbhum Craton is enormously rich in mineral resources, particularly iron and copper, with a geological history including Archean metamorphic rocks, volcano-sedimentary sequences, and sedimentary layers, providing crucial insights into continental crustal development and the Archean Earth processes. It features a central granitic batholith surrounded by greenstone belts that contain various types of volcanic and sedimentary rocks. The Singhbhum Craton located in Peninsular India, hosts significant ultramafic complexes, such as the Sukinda and Baula-Nuasahi complex, which are important for their hosted chromite and PGE deposits. These layered ultramafic bodies, consisting of rocks like dunite, pyroxenite, gabbro and serpentinite, that are found within the Archaean Iron Ore Group (IOG) of volcano-sedimentary successions. The southern marginal zone of the Singhbhum Craton boarders with EGMB, encompassing chromite hosted layered ultramafic bodies (Figure 1a). Apart from the prominent ultramafic complexes like the Baula-Nuasahi Ultramafic Complex (BNUC) and the Sukinda Ultramafic Complex (SUC), there is some recently identified ultramafic complex, like the Bhuban Ultramafic Complex (BUC) in the Dhenkanal district of Odisha (Tripathy et al., 2014). The BUC forms part of the transition zone between the Singhbhum Craton and the EGMB, which exposes rocks belonging to cratonic fringe as well as the granulites (Figure 1b). The northern margin of EGMB against the Singhbhum Craton, distinctly considered as a strike-slip fault or exposing the deeper crustal segment of the Archean crust through oblique transpression, represents a complex geological setting (Mishra and Gupta, 2013).

A number of small chromiferous ultramafic bodies occur towards southeast of the SUC within the granulite terrains north of the Maulabhanja Parbat towards the west and Asurabandh towards the east (Banerjee et al., 1972). Another small chromiferous ultramafic body occurs further east of Asurabandha nearby Bhuban. All these three dismembered chromiferous ultramafic units are clubbed together and here after called as the Bhuban Ultramafic Complex (BUC). The stratigraphic corelation between BUC with respect to the SUC and the BNUC remains speculative. Asurabandha area is characterized by ultramafic bodies containing chromite, which are found within the less-understood granulite tracts near the SUC (Figure 1b). These ultramafic rocks are partially covered by a thick laterite overburden. Geological studies have utilized gravity and magnetic surveys to investigate the concealed chromite mineral potential of the Asurabandha - Bhuban area (Arasada et al., 2020). The BUC is characterized by the emplacement of a number of lensoidal bodies of chromiferous ultramafic rocks. Layered mafic-ultramafic rocks represented by dunite, peridotite, and gabbro occurs as lenses within granite-charnockite association along the transition domain between the Singhbhum Craton and the EGMB. In the study area, lensoidal chromite bearing rocks are highly prone to alteration and weathering as well as extend beyond lateritic overburden. The Bhuban-Asurabandha area is represented by low physiographic terrain. A number of old working pits are located in this area around three different localities nearby Chandar, Bhuban and Maulabhanja Parbat areas (Tripathy et al., 2014).

In Asurabandha area, the ultramafic complex has experienced widespread lateritization and serpentinization to several stages of hydrothermal alterations. Apart from the chromite-bearing weathered peridotite, the other ultramafic or mafic rocks include gabbro, pyroxenite, anorthosite and gabbroic-anorthosite (Figure 2a). In spite of restricted exposures, they form essential components of a magmatic suite of rocks. The ultramafic body occurred in the form of chromite-bearing weathered peridotite, gradually transit close to gabbro and anorthositic-gabbro. The compositional variation is observed only in a few metres wide exposed outcrops. These bodies are circular to semi-circular or elliptical in nature. The ultramafic rocks like dunite, peridotite, serpentinite and silicified serpentinite bodies with chert and chromite occurs as discrete isolated bodies in the granitic-charnockite terrain. They do not show any regularity, either in distribution pattern or in concentration of chromite. Chromite is found in irregular form and in small dimensions with massive, spotted and banded varieties (Figure 2b). The silica veins traversing serpentinite are quite frequently observed in this area. At several places, the ultramafic rocks have been altered to chrysotile asbestos, which is green colour, hard compact and light in weight. Relatively, fresh samples of peridotites consist of olivine and enstatite with magnetite, chromite, and apatite as accessories. The dunite is altered to a felted mass of talc-serpentine.

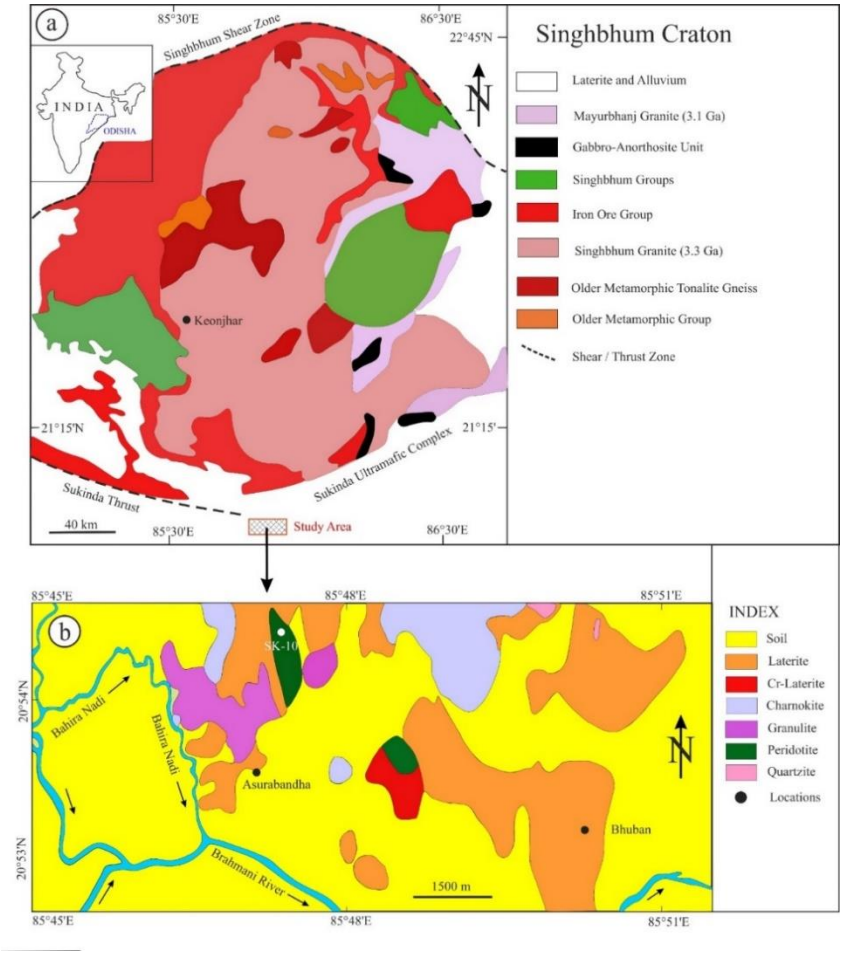


Figure 1. (a) Generalised geological map of the Singhbhum Craton (after Saha, 1994) and its adjacent areas with an inset of map of India displaying study area in Odisha. The cross-hatched red colour box is shown to represents the study area of the Bhuban Ultramafic Complex (BUC). **(b)** Geological map of Asurabandha chromite deposits of the BUC in Dhenkanal district of Odisha (modified after Sahoo, 2014; Tripathy et al., 2014; Arasada et al., 2020; Behera and Nayak, 2023).

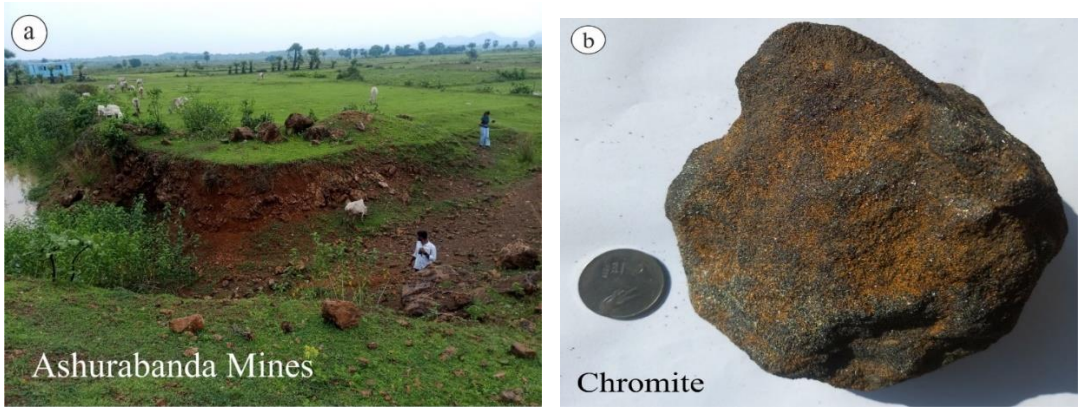


Figure 2. (a) Field photograph showing exposed area of the Asurabandha Chromite Mines. **(b)** Hand specimen of chromite sample from the Asurabandha Mines in Dhenkanal district of Odisha. The metallic lustre with well-developed granular texture is a diagnostic feature of magmatic chromite ore. The chromite ore exhibits secondary alteration features of serpentine and goethite.

SAMPLE PREPARATION

A small piece of rock is cut, ground to a smooth surface, and then pasted to a glass slide. The mounted rock slice is then ground down to a very thin layer using progressively finer abrasive grits and water, often with the aid of specialized grinding machines. This step continues until the desired thickness of approximately 30 micrometers is achieved. Excess

material is removed to create a thin slice, allowing light to pass through. Grinding of the sample to a precise thickness of about 30 micrometers is done using progressively finer abrasives, and then by systematic polishing. The sample surface is then polished to a smooth and flat appearance. The prepared thin section is used for petrographic study under a polarized-light microscope to identify its constituent minerals, texture, and structure. Microscopic study of the thin section is performed in the Department of Geology, Institute of Science, Banaras Hindu University, India. Mineral identification by rotating the polarizing filters attached with the microscope, that can identify individual minerals based on their unique optical properties, such as colour, birefringence, and crystal shape. Texture and fabric analysis consists of the arrangement, shape, and size of mineral grains, as well as any cracks or other structural features.

PETROGRAPHY

The chromite ores from the Asurabandha area are examined under thin section using a petrological microscope. These samples show cumulus texture formed by 70 to 90% euhedral chromite grains in an altered and silicified matrix comprising of serpentine group of minerals. In plane polarized transmitted light (PPTL) mode, chromite (opaque grains) in ultramafic rocks display massive, disseminated, or granular textures, with grains often exhibiting euhedral to subhedral shapes and intergrown with interstitial serpentine (pale yellow colour) or olivine's remnant (Figure 3a). Grains may form compact mosaics, chains, or clots. In cross polarized transmitted light (XPTL) mode, chromite appears as opaque grains surrounded by interstitial silicate matrix of serpentine typically appearing as an anisotropic mineral with low first-order interference colours (Figure 3b). Serpentine displays black, white, and grey hues with sweeping undulose extinction. Under plane polarised reflected light (PPRL) mode, the chromite grains show fractures, filled up with secondary silicate matrix (Figure 3c). The chromite grains contain very fine inclusions of silicate matrix. The shape of the chromite grains varies from hexagonal, euhedral to subhedral and size varies from 10 to 500 µm recognised as heteradcumulate texture. It shows heterogeneous distribution of the chromite crystal aggregates in the ultramafic rocks of the Asurabandha chromite deposit. A heteradcumulate texture represents euhedral to subhedral chromite grains that are surrounded by inter-cumulus minerals, such as serpentine or olivine (Wager et al., 1960; Campbell, 1978). The dunite is altered to talc-serpentine rock, often preserving ghost heteradcumulate texture, formed by hexagonal pseudomorphs of chromite having rims of released iron rich secondary mineral phases (Figure 4a**).** In XPTL mode, the chromite grains, although opaque phase, are interpreted on the basis of hexagonal shape and surrounding silicate matrix of serpentine (Figure 4b). In PPRL mode, chromite grains are appearing as perfect hexagonal crystallized grains with white colour interstitial spaced filled by silicate matrix of serpentine (Figure 4c). There are some secondary mineral phases filled in the fractures that facilitated alteration displayed as pale-green colour hues most probably goethite. Altered peridotite with preserved pyroxene and chromite cumulates are sometimes observed under XPTL mode with imprints of metasomatism and post alteration patterns of serpentinization and carbonation. This alteration process, recognized as serpentinization or hydrothermal alteration, involves the interaction of the hot, mineral-laden fluids with the chromite, causing the chromium to become incorporated into new carbonate minerals (Kraemer et al., 2021). Hydrothermal alteration, prevalent in serpentinization and low to mid-amphibolite facies metamorphism, results in the breakdown of the primary chromite structure and the redistribution of Mg and Al, ultimately changing the chromite's chemical composition and creating zoned alteration rims (Barnes, 2000; Santti et al., 2006). Carbonation of chromite is a dissolution-precipitation process, where metals in chromite react with carbon dioxide (CO_2) in presence of mineralising fluids to form carbonate minerals (Ashwal and Cairncross, 1997).

LASER RAMAN MICRO SPECTROSCOPY: THEORY AND METHODOLOGY

The Raman effect is a phenomenon where monochromatic light (like laser light) interacts with a substance, causing a small fraction of the light to be scattered at a different frequency, or wavelength (Raman, 1922, 1923). The Raman scattering is the inelastic scattering of photons by a molecule, where the radiation or photon's energy is either gained or lost by the molecule or crystals, resulting in a scattered photon with a different energy (frequency) than the incident radiation or photon (Raman, 1928, 1929). This process occurs when incident monochromatic light (like from a laser) interacts with a molecule, exciting it to a temporary virtual energy state, and then the molecule relaxes back to a vibrational state, releasing a radiation or photon (Raman, 1942, 1943). A laser beam shines onto the sample, exciting molecules into a virtual energy state, the molecules relax, most photons are scattered elastically (Rayleigh scattering) with the same energy. However, a small fraction undergoes inelastic scattering (Raman scattering), where the scattered photon's energy (and thus its frequency) is shifted up or down (Raman, 1945, 1947). The variance in energy amongst the incident and scattered photons, provides a unique "fingerprint" of the molecule's vibrational modes, which can be used for material identification and characterization (Neuville et al., 2014). The variance in frequency amongst the incident and scattered light is recognized as the Raman Shift, which factor is measured in cm^{-1} unit. A spectrometer analyses the intensity of these scattered photons at different Raman Shifts, producing a unique spectrum that acts as a "fingerprint" for the sample.

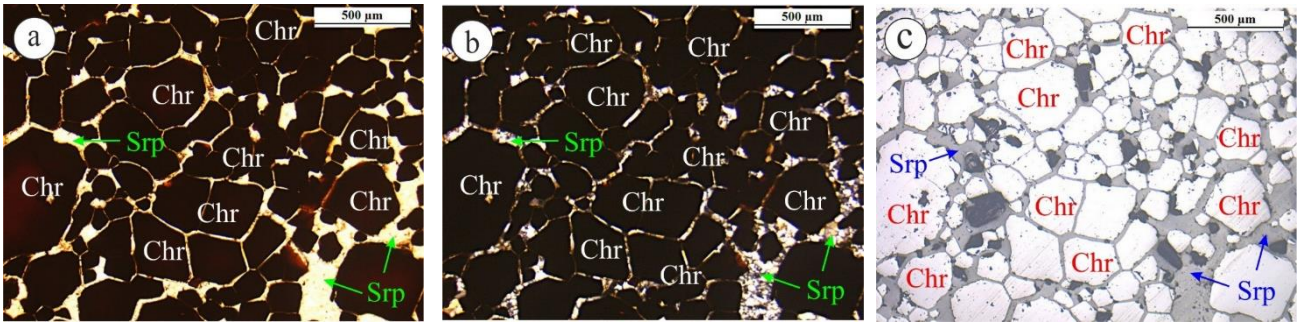


Figure 3. Photomicrograph (5X magnification) of chromite in ultramafic rock from the Asurabandha Mines in Dhenkanal district of Odisha. In ultramafic rock, euhedral and subhedral chromite grains are commonly displays heteradcumulate textures, with silicate minerals (serpentine) filling the interspaces between the grains**. (a)** In plane polarized transmitted light (PPTL) mode, chromite-serpentine matrix is shown as serpentine colourless whereas chromite appears as black under**. (b)** In cross polarized transmitted light (XPTL) mode, chromite shows black colour and serpentine exhibits grey colour. **(c)** In plane polarized reflected light (PPRL) mode, chromite crystals show white colour and serpentine-silicate matrix displays grey-black colour. Chr - chromite, Srp - serpentine.

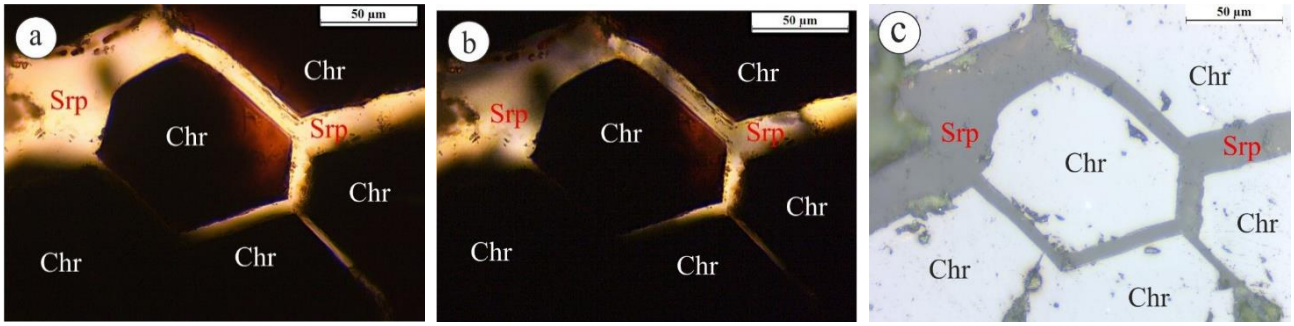


Figure 4. Photomicrograph (50X magnification) of chromite in ultramafic rock from the Asurabandha Mines in Dhenkanal district of Odisha. Serpentine occurs as packing the interspaces between the chromite grains**. (a)** Under PPTL mode, chromite appears as opaque with euhedral, hexagonal shape crystals and serpentine exhibits pale-yellow to colourless. **(b)** Under XPTL mode, serpentine exhibits pale-yellow colour and chromite is opaque**. (c)** Under PPRL mode, chromite appears as white colour, euhedral hexagonal shape crystals, serpentine displays grey colour and secondary minerals (goethite) show green colour along the interspaces between chromite crystals. Chr - chromite, Srp - serpentine.

The LRMS is a non-destructive technique that uses a laser and microscope to analyse the vibrational spectrum of a sample's molecules, providing a chemical "fingerprint" with high spatial resolution (around 1 µm). It works by analysing inelastic (Raman) light scattering, where the energy of the light changes due to interactions with the sample's molecular vibrations. The LRMS combine with a Scanning Near-field Optical Microscopy (SNOM) instrument is to circumvent the diffraction limit of conventional light microscopy by using a subwavelength-sized aperture or tip to probe the near-field of the sample (Vandenabeele, 2013). This integration permits for the acquisition of topographic and chemical information on the surface characterization of minerals at the nanoscale investigations (>100 nm). By scanning Raman-SNOM probe across a sample surface at a close distance, the technique collects optical information, such as transmitted, reflected, or fluorescent light, by exploiting evanescent waves or tip-scattered light. This allows for the simultaneous imaging of topography and optical properties with high spatial resolution, making it useful in fields like nanotechnology, geology, and materials science. The detail procedure of mineral characterization using the Raman-SNOM probe is performed at the Central Discovery Centre (CDC), Banaras Hindu University, India (Pandit, 2024). Raman spectral mapping is a hyperspectral imaging technique that provides detailed chemical and structural information by acquiring a full Raman spectrum at every pixel of an image. Using Laser Raman 2D and 3D mapping distinctions in these spectra. This technique creates false-colour images that reveal the spatial distribution of different chemical components within a sample, allowing for the visualization of features invisible to standard optical microscopy. The RRUFF database contains Raman spectra, and chemistry data of minerals, offering a powerful tool for their identification (Lafuente et al., 2015). This software assists in analysing and identifying minerals by comparing collected spectra to those available in the RRUFF website (https://rruff.info/).

RESULTS

The Laser Raman-SNOM system (MakeWITec, GmbH, model: alpha 300-RAS) attached with 532 nm wavelength laser beam using a solid state Nd:YAG crystal operated through output power 0.3 to 1 mW. The analytical resolution of Raman-SNOM instrument can range from 2 to 4 cm^{-1} for routine data

acquisition, covering full spectral range from 100 to 3500 cm^{-1} with an accuracy of ±5cm^{-1} or even higher. The Raman spectra were acquired from chromite crystal and surrounding silicate phase or matrix, using 532 nm wavelength excitation laser which is focused on polished thin sections of ultramafic rock sample (Figure 5a).

The grey colour silicate matrix of serpentine is recognized by five indicative Raman Shifts at around 127, 206, 397, 465 and 1166 cm^{-1} (Figure 5b). Serpentine is a Mg-Fe-rich layered silicate mineral group [nominally $(Mg,Fe)_3Si_2O_5(OH)_4$] with three distinct polymorphs such as antigorite, chrysotile and lizardite (Aspiotis et al., 2023). The Raman Band or Shift at ~128 cm^{-1} is attributed to the doubly degenerate vibration E-mode and Raman Shift at ~206 cm^{-1} attributed to the Raman active symmetric A1-mode stretching style vibration of the SiO_4-tetrahedra crystal structure of four membered framework rings (Liu et al., 1997; Li et al., 2025). A Raman Shift at ~397 cm^{-1} in serpentine suggests the presence of the lizardite polymorph, which exhibits a characteristic peak in the silicate matrix (Bahram et al., 2019). The strong Raman Shift at ~465 cm^{-1} in silicate matrix is a characteristic vibrational mode resulting from the symmetric Si-O-Si stretching-bending within the silica ring structures (SiO_4-tetrahedra framework), indicating the presence of quartz crystal (Gillet et al., 1990). A weak Raman Shift at ~1166 cm^{-1} in the silicate structure can be accredited to the symmetric stretching vibration of (Si-O-Si) silicon-oxygen bonds, specifically from a non-bridging oxygen of silicate tetrahedra within a glass or silicate framework (McMillan, 1984). While prominent Si-O-Si stretching bands are typically in the 850–1150 cm^{-1} range, a peak at this specific wavenumber suggests a particular configuration of the silicate network structure (White and Minser, 1984).

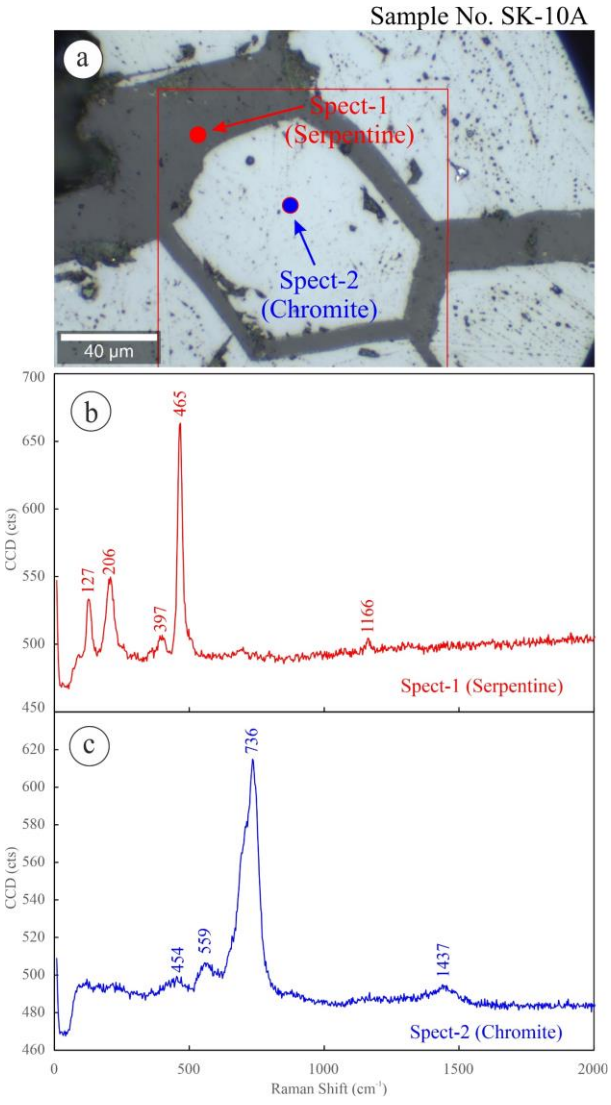


Figure 5. (a) Representative photomicrograph display chromite grain in the silicate phases or matrix of ultramafic rock. Characteristic Raman spectra of **(b)** silicate matrix (serpentine), and **(c)** chromite crystals in the silicate matrix of the ultramafic rock from the Asurabandha Chromite Mines in Dhenkanal district of Odisha.

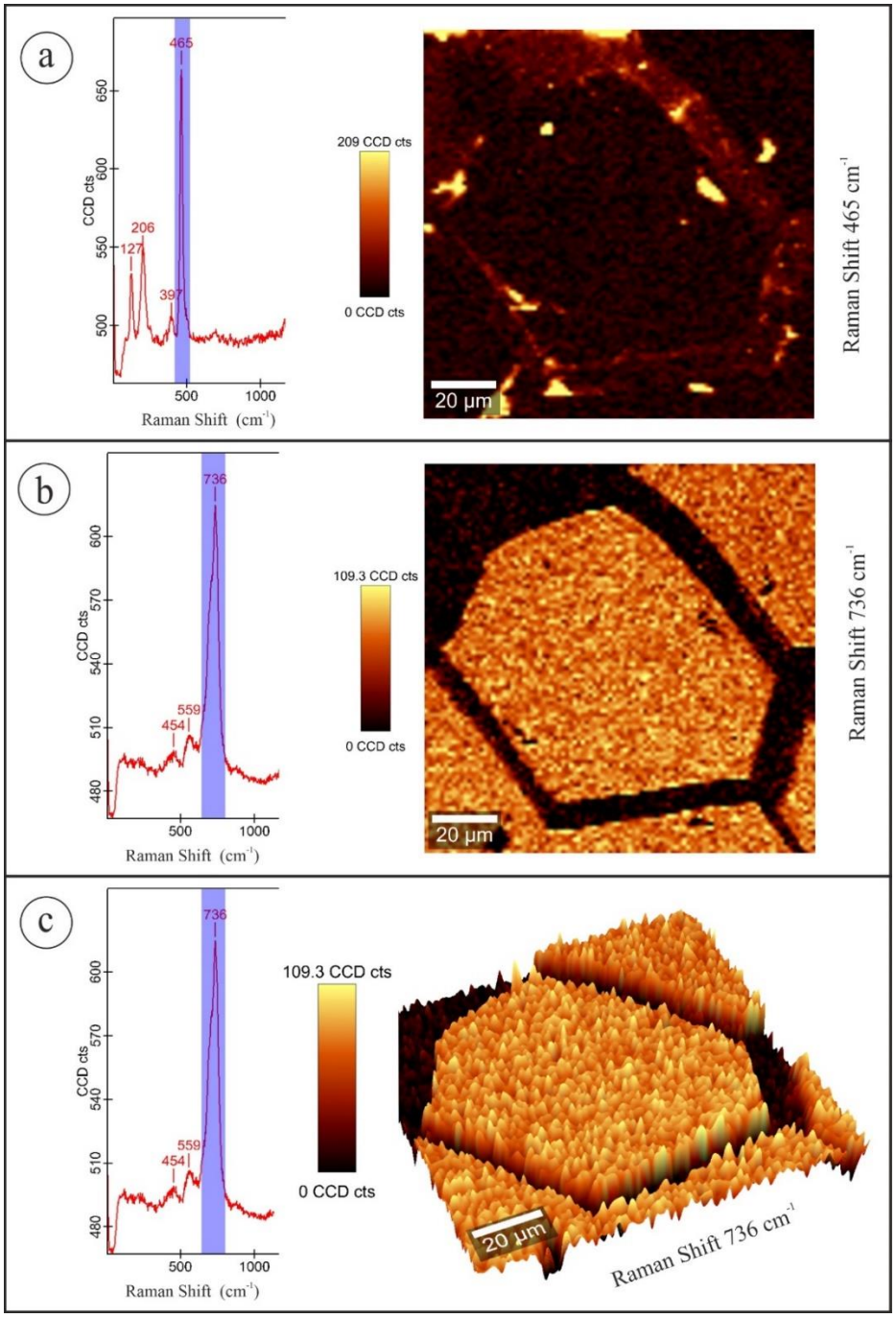


Figure 6. Laser Raman mapping of mineral phases in ultramafic rock from the Asurabandha Chromite Mines in Dhenkanal district of Odisha. **(a)** Raman spectrum of silicate matrix with 2D mapping over Raman Shift 465 cm^{-1}, **(b)** Raman spectrum of chromite crystal with 2D mapping over Raman Shift 736 cm^{1} and **(c)** Raman spectrum with 3D mapping over Raman Shift 736 cm^{-1} for euhedral chromite crystal in the ultramafic rock.

The white colour euhedral chromite crystal ($FeCr_2O_4$ or $FeO.Cr_2O_3$), is characterized by four significant Raman Shifts at approximately 454, 559, 736 and 1437 cm^{-1} (Figure 5c). A weak Raman Shift ~ 454 cm^{-1} in chromite is typically assigned to the E(g) vibrational modes, which are generally represents a minor Raman peak at lower wavenumbers compared to the strong A_1g mode at 680-730 cm^{-1} (Kharbish, 2018). The intensity and exact position of this Raman Shift are influenced by cation substitutions within the chromite's spinel lattice, particularly Fe^{3+} and Al^{3+} (Lughi et al., 2020). The presence of a Raman Shift ~559 cm^{-1} is typically attributed to the F_2g, may be due to impurities or the formation of chromium-bearing phases from the degradation of chromite, such as ferrian chromite (Reddy and Frost, 2005; Zhang and Gan, 2011) or manganese-substituted chromite (Ha et al., 2025). In the Raman spectrum of chromite, the most intense Raman Shift at

~736 cm^{-1} corresponds to the A_1g symmetric stretching mode of the Cr-O bonds within the octahedral groups (Nestola et al., 2014). Chromite is a solid solution with the spinel structure (AB_2O_4) where different cations (Fe^{2+}, Mg^{2+}, Cr^{3+}, Al^{3+}) can substitute for each other (Bosi et al., 2019). A very weak Raman Shift at ~1437 cm^{-1} is typically assigned to the carbonate (CO_3^{2-}) group that appears due to the symmetric stretching vibration mode (Gunasekaran et al., 2006), which indicates presence of carbonate rich mineral phases in the chromite crystals. Low-temperature, carbonate-rich fluids can alter chromite, a chromium-bearing mineral, into a hydrous chrome carbonate through chemical reactions that replace the original crystal structure in the ultramafic rocks (Klein and Garrido, 2011; Majumdar et al., 2016).

DISCUSSION

Chromite is an accessory mineral in mafic rocks but it becomes a dominant mineral in chromitite, often found in ultramafic rocks and coexists in serpentinites (Irvine, 1965; Burkhard, 1993). Chromite is the principal chromium ore, forming as an early-crystallizing mineral in ultramafic rocks like dunite, peridotite, and their secondary product as serpentinite within layered igneous complexes and ophiolites (Stowe, 1994). It occurs in various forms, such as disseminated grains, bands, lenses, and pockets. In Asurabandha chromite deposits, chromite grains are linked and compact, forming a mosaic, chain, or net-like texture in the ultramafic rock. The magmatic texture is the ultramafic rock where cumulus chromite grains form a dense, interconnected framework, and the inter-cumulus minerals (serpentine) fill the spaces between them, which is representative of adcumulate, heteradcumulate, and harrisitic-cumulate types (Wager et al., 1960). In general, cumulus texture in chromitite rocks signify to euhedral to subhedral chromite crystals that settle from a crystallizing magma, forming a framework that encloses later-crystallizing inter-cumulus minerals like serpentine, olivine, or pyroxene termed as heteradcumulate texture (Wager, 1959). Heteradcumulate textures in chromite are characterized by a rock composed almost entirely of poikilitic oikocrysts, which are larger crystals that enclose smaller, cumulus crystals, with little to no inter-cumulus matrix (Campbell, 1968; Hunter, 1996). These textures develop from in-situ crystallization within a boundary layer between a crystal mush and evolving magma. Their formation is favoured by a lack of cumulus seeds in the presence of supercooled magma (Barnes, 1986; Tegner and Wilson, 1995). Various types of cumulus textures are characteristic features of chromitite, a heteradcumulate texture consisting of chromite grains (oikocrysts) that enclose other cumulus minerals like olivine or pyroxene, which then crystallize within interstitial spaces (Campbell, 1978; Latypov et al., 2017). The heteradcumulate texture forms when larger chromite crystals grow from a supersaturated magma, capturing smaller, pre-existing minerals within their structure as they crystallize in place, rather than as a result of direct gravity-induced settling (Tait et al., 1984; Latypov et al., 2022).

Nucleation and crystal growth process is crucial in determining the magmatic texture and crystallization sequence of basaltic or ultramafic rocks, as the foreign surfaces reduce the supercooling or undercooling required for a stable crystal nucleus to form (Gray, 1970; Brandeis et al., 1984; Toramaru and Kichise, 2023). Crystal nucleation in basaltic magma involves the spontaneous formation of crystals or gas bubbles within the bulk of the liquid magma, without the help of existing surfaces or defects (Berkbile and Dowty, 1982; Polacci et al., 2018). Homogeneous and heterogeneous nucleation in basaltic magma involves solid crystals forming on the surfaces of seed grains, which is a more likely process than homogeneous nucleation due to the lower energy barrier (Lofgren, 1983; Gonnermann and Gardner, 2013; Shea, 2017). Common nucleation centres in natural basaltic magmas include other minerals (like pyroxene or olivine), suspended crystals, and even microscopic bubbles, significantly impacting the magma's behaviour during crystallization and evolution of igneous microstructures (Donaldson, 1979; Hersum and Marsh, 2006; Hammer et al., 2010). Euhedral chromite crystals can origin in ultramafic or basaltic magma, but their final appearance depends on the magma's cooling rate and stages of chemical differentiation (Holness et al., 2023). As one of the first minerals to crystallize in the ultramafic magma, chromite can be either euhedral, granular, nodular or dendritic (branching) depending on whether crystal growth is slow or rapid, which depends on the physical process of nucleation (Henry et al., 2024). Chromite crystallization occurs when a chromium-bearing mafic or ultramafic magma becomes immiscible system with olivine and pyroxene, and is heavily influenced by geochemical composition, oxygen fugacity, and the presence of other minerals (Roeder and Reynolds, 1991). As the magma cools, the liquidus of descent follows the chromite saturation surface, when chromium saturation is achieved in the ultramafic magma, it results in the crystallization of chromite (Murck and Campbell, 1986). At the early stage in the process of basaltic magma crystallization, the parental magma (often mafic or ultramafic) cools, leading to the crystallization of early-forming chromite crystals (Barnes, 1986; Latypov et al., 2022). The accumulation of these chromite crystals can form layers of chromitite, a type of rock composed almost entirely of chromite with minor silicate matrix between interstitial mineral grains.

Alteration of ultramafic rocks is primarily known as serpentinization, carbonation and metasomatism, the process where primary magnesium-rich minerals like olivine and

pyroxene are replaced by hydrous minerals, especially serpentine (Moody, 1976; McCollom and Bach, 2009; Klein et al., 2013). In general, serpentinization, which involves water-bearing fluids can lead to carbonation, silicification, that result production of hydrogen gas, impacting the rock's density, magmatic texture and primary mineralogy (Schwarzenbach et al., 2021; Hu et al., 2025). Carbonation of chromite during serpentinization involves the reaction of carbon dioxide (CO_2)-bearing fluids with serpentinized magmatic rocks, including those containing chromite, to form carbonate minerals like magnesite and/or dolomite (Klein et al., 2013; Huang et al., 2024). Formation of carbonate minerals due to carbonation process of chromite, typically occurring in mafic and ultramafic rocks, leads to changes in mineralogy and fluid chemistry (Klein and Garrido, 2011). As divalent cations in mafic and ultramafic rocks like magnesium, iron, and calcium bind with CO_2 results in the formation of carbonate minerals such as pyroaurite, stichtite and manasseite (Frondel, 1941). Carbonate-rich fluids cause chromite alteration by driving Mg-Fe exchange and Al loss, leading to the formation of iron-rich ferritchromite or ferrichromite and associated silicates like antigorite (Hodel et al., 2020; Eberhard et al., 2023). The specific conditions of the hydrothermal fluids, such as their temperature, pressure, and chemical composition, influence the type and extent of alteration encompass metasomatism, serpentinization and carbonation processes. The serpentinization and carbonation reactions are often associated with seafloor hydrothermal systems and subduction zones (Lowell and Rona, 2002; Deschamps et al., 2013). Alteration of ultramafic rocks lead to changes in the mineralogy, porosity, and chemical composition of the rocks, with potential effects on the solubility and redistribution of elements like chromium within the system (Oze et al., 2004; Shen et al., 2021). Serpentinization alters chemical composition of chromite crystal by reacting with carbonate-rich fluids, causing mineralogical changes like ferrichromite, pyroaurite, stichtite and can incorporate various trace elements (Sc, Ti, V, Ni, Mn, Co, and Zn) enrichment at earlier stages (Ulmer, 1974; Bara et al., 2014; Datta and Mondal, 2021; Liu et al., 2023).

In the Asurabandha chromite deposit, euhedral chromite crystals growth suggested that the magmatic conditions allow for uninhibited and sustained crystallization in a state of moderate super-saturation. This is more common in large, slow-cooling layered intrusions, to develop fully-formed crystal faces, chromite needs the right balance of heat, chemical supply, and physical space. Slow cooling rate provides sufficient time for the atoms of a mineral to migrate through the magma and systematically attach to the surfaces of a crystal growth. The surrounding magma must continuously resupply the elements needed to build the crystal structure of chromite, in this case, magnesium (Mg), iron (Fe), chromium (Cr) and aluminium (Al) supply from the magma. However, the Laser Raman-SNOM application with 2D (Figure 6a, b) and 3D mapping (Figure 6c) of chromite crystal from the Asurabandha deposits, indicates inhomogeneous or heterogeneous pattern observed in the chromite crystal structure. The chromite crystal is described as heterogeneous because its chemical composition is highly variable, and its internal crystal structure can be complex, possibly influenced by the crystallization conditions under which it formed or may be affected by hydrothermal alteration processes.

CONCLUSIONS

In Asurabandha deposits, chromite may be crystallized through heterogeneous nucleation in ultramafic magma, where new crystals grow on existing ones, resulting in aggregated or clustered textures. The crystal nucleation may be random rather than following a precise crystallographic alignment, further contributing to the heterogeneous distribution of the chromite crystal aggregates. This results in the heteradcumulate-like appearance where chromite crystals grown surrounded by silicate matrix. A chromite heteradcumulate texture is a type of igneous cumulate texture, where, large interlocking crystals of chromite (the cumulus minerals) enclose smaller, randomly oriented silicate crystals, such as olivine or pyroxene, that later altered to serpentine. The heteradcumulate texture observed in the Asurabandha chromite deposit inferred the specific arrangement where the cumulus minerals (chromite) have overgrown to enclose the inter-cumulus grains. The heteradcumulate texture of chromite crystal indicates a specific sequence of magma crystallization and evolution. Early crystallization, during the cooling of a magma, chromite begins to crystallize at a high temperature and accumulates to form a framework of crystals. Growth of surrounding crystals, the interstitial melt, trapped between the chromite grains, subsequently crystallizes to form silicate minerals like olivine or pyroxene.

In Asurabandha chromite deposits, presence of euhedral chromite crystal is a strong evidence that an individual grain of the mineral which crystallized without any interference, well-defined crystal faces reflect its inherent crystal structure. However, the Laser Raman-SNOM studies infer that the euhedral chromite phases are heterogenous with respect to internal crystal structure. The internal structure of chromite crystal and chemical composition are non-uniform. In chromite grain, heterogenous crystal structure are referring to primary characteristics with two distinct properties: (i) variable chemical composition in the crystal, and (ii) different processes of nucleation that favour crystal growth during crystallization in the magma. Compositional heterogeneity in the chromite crystal may appear because of trace element substitution during magmatic crystallization or secondary alteration processes.

Acknowledgements

The authors acknowledged to the Head of the Department, Department of Geology, Institute of Science, Banaras Hindu University (BHU) for providing necessary facilities. AG acknowledged the Council of Scientific & Industrial Research (CSIR), New Delhi, sponsored Junior Research Fellowship. DP acknowledged financial support from BHU Institute of Eminence (IoE) sponsored SEED Grant and Professional Development Fund (PDF).

Author credit statement

AG: Data curation, data analysis methodology, preparation of maps, editing and processing of complete data. This work is a part of his doctorate thesis, DP: conceptualization, data curation, quality checks, methodology, funding acquisition, draft editing and revision and supervision.

Data availability

Data is presented in the article.

Compliance with ethical standards

The authors declare that there is no conflict of interest and adhere to copyright norms.

References:

Arasada, R.C., Srinivasa Ra., G. and Sahoo, P.R., 2020. Integrated geological and geophysical studies for delineation of laterite covered chromiferous ultramafic bodies around Bhuban, southwestern part of Sukinda ultramafic complex, Odisha. Ore Geol. Rev., 119, 103402. https://doi.org/10.1016/j.oregeorev.2020.103402.

Ashwal., L.D. and Cairncross, B., 1997. Mineralogy and origin of stichtite in chromite-bearing serpentinites. Contrib. Mineral. Petrol., 127, 75-86.

Aspiotis, S., Schluter, J., Hildebrandt, F. and Mihailova, B., 2023. Raman spectroscopy for crystallochemical analysis of Mg-rich layered silicates: serpentine and talc. J. Raman Spectrosc., 54(12), 1502-1516.

Bahram, B., Hesam, M., Prakash, D. and Iris, W., 2019. Raman characteristics of Alpine–Himalayan serpentine polymorphs: A case study of Khankuie ultramafic complex, southeast of Iran. J. Earth Syst. Sci., 128, 238. https://doi.org/10.1007/s12040-019-1259-6.

Banerjee, P.K., 1972. Geology and Geochemistry of the Sukinda Ultramafic Field, Cuttack district, Orissa. Mem. Geol. Surv. Ind., 103, 1-320.

Barnes, S.J., 1986. The effect of trapped liquid crystallization on cumulus mineral compositions in layered intrusions. Contrib. Mineral. Petrol., 93, 524-531.

Barnes, S.J., 2000. Chromite in komatiites, II. modification during greenschist to mid-amphibolite facies metamorphism. J. Petrol., 41(3), 387-409.

Barra, F., Gervilla, F., Hernández, E., Reich, M., Padron-Navarta, J.A. and Gonzalez-Jimenez, J.M., 2014. Alteration patterns of chromian spinels from La Cabaña peridotite, south-central Chile. Miner. Petrol., 108, 819-836.

Behera, A. and Nayak, B., 2023. Metasomatic silicification of chromitite bodies in Asurabandha area, Odisha, India. J. Earth Syst. Sci., 138, 148. https://doi.org/10.1007/s12040-023-02167-1.

Berkebile, C.A. and Dowty, E., 1982. Nucleation in laboratory charges of basaltic composition. Am. Min., 67, 886-899.

Bersani, D. and Lottici, P.P., 2016. Raman spectroscopy of minerals and mineral pigments in archaeometry. J. Raman Spectrosc., 47, 499-530.

Bosi, F., Biagioni, C. and Pasero, M., 2019. Nomenclature and classification of the spinel supergroup. Eur. J. Mineral., 31, 183-192.

Brandeis, G., Jaupart, C. and Allegre, C.J., 1984. Nucleation, crystal growth and the thermal regime of cooling magmas. J. Geophys. Res., 89, B12, 10161-10177.

Burkhard, D.J.M., 1993. Accessory chromium spinels: their coexistence and alteration in serpentinites. Geochim. Cosmochim. Acta, 57, 1297-1306.

Campbell, I.H., 1968. The origin of heteradcumulate and adcumulate textures in the Jimberlana norite. Geol. Mag., 105(4), 378-383.

Campbell, I.H., 1978. Some problems with the cumulus theory. Lithos, 11, 311-323.

Datta, P. and Mondal, S.K., 2021. Compositional variations, thermometry, and probable parental magmas of Archean chromite from the Sargur greenstone belt, Western Dharwar Craton (India). Lithos, 380-381, 105867. https://doi.org/10.1016/j.lithos.2020.105867.

Deschamps, F., Godard, M., Guillot, S. and Hattori, K., 2013. Geochemistry of subduction zone serpentinites: A review. Lithos, 178, 96-127.

Donaldson, C.H., 1979. An experimental investigation of the delay in nucleation of olivine in mafic magma. Contrib. Mineral. Petrol., 69, 21-32.

Eberhard, L., Frost, D.J., McCammon, C.A., Dolejs, D. and Connolly, J.A.D., 2023. Experimental constraints on the ferric Fe content and oxygen fugacity in subducted serpentinites. J. Petrol., 64, 1-18.

Frondel, C., 1941. Constitution and polymorphism of the pyroaurite and sjogrenite groups. Am. Min., 26, 295-315.

Gillet, P., Cleach, A.L. and Madon, M., 1990. High-temperature Raman Spectroscopy of SiO_2 and GeO_2 polymorphs: anharmonicity and thermodynamic properties at high temperature. J. Geophys. Res. Solid Earth, 95, 21635-21655.

Gonnermann, H.M. and Gardner, J.E., 2013. Homogeneous bubble nucleation in rhyolitic melt: Experiments and nonclassical theory. Geochem. Geophys. Geosyst., 14, 4758-4773.

Gray, N.H., 1970. Crystal growth and nucleation in two large diabase dikes. Can. J. Earth Sci., 7(2), 366-375.

Gunasekaran, S., Anbalagan, G. and Pandi, S., 2006. Raman and infrared spectra of carbonates of calcite structure. J. Raman Spectrosc., 37, 892-899.

Ha, D.H., Noh, G., Kim, H., Kim, D.H., Kim, J., Jung, S., Hwang, C., Lee, H.Y., Yun, Y.J., Kwak, J.Y., Kang, K. and Yi, S.N., 2025. Raman spectroscopy study of K-birnessite single crystals. J. Mater. Chem. A, 13, 617. https://doi.org/10.1039/D4TA06118G.

Hammer, J.E., Sharp, T.G. and Wessel, P., 2010. Heterogeneous nucleation and epitaxial crystal growth of magmatic minerals. Geology, 38(4), 367-370.

Henry, H., Ceuleneer, G., Proietti, A., Kaczmarek, M.A., Chatelin, T. and De Parseval, P., 2024. How does nodular chromite nucleate and grow? an integrated microstructural and petrological approach. J. Petrol., 65, egae061. https://doi.org/10.1093/petrology/egae061.

Hersum, T.G. and Marsh, B.D., 2006. Igneous microstructures from kinetic models of crystallization. J. Volcan. Geoth. Res., 154, 34-47.

Hodel, F., Macouin, M., Trindade, R.I.F., Araujo, J.F.D.F., Respaud, M., Meunier, J.F., Cassayre, L., Rousse, S., Drigo, L. and Schorne-Pinto, J., 2020. Magnetic properties of ferritchromite and Cr-magnetite and monitoring of Cr-spinels alteration in ultramafic and mafic rocks. Geochem. Geophys. Geosyst., 21, e2020GC009227. https://doi.org/10.1029/2020GC009227

Holness, M.B., Vukmanovic, Z. and O'Driscoll, B., 2023. The formation of chromite chains and clusters in igneous rocks. J. Petrol., 64, 1-24.

Hope, G.A., Woods, R. and Munce, C.G., 2001. Raman microprobe mineral identification. Min. Eng., 14, 1565-1577.

Hu, Z., Qin, M., Xing, H., Wang, J., Jin, G., Tan, Y. and Yan, W., 2025. Effects of serpentinization and deserpentinization on rock elastic properties in subduction zones. Earth Sci. Rev., 263, 105069. https://doi.org/10.1016/j.earscirev.2025.105069.

Huang, Y., Okumura, S., Matsumoto, K., Takahashi, N., Tang, H., Wu, G., Tsujimori, T., Nakamura, M., Okamoto, A. and Li, Y., 2024. Experimental constraints on serpentinite carbonation in the presence of a H_2O–CO_2–NaCl fluid. Contrib. Mineral. Petrol., 179, 98. https://doi.org/10.1007/s00410-024-02175-4.

Hunter, R.H., 1996. Texture development in cumulate rocks. Developments in Petrology, 15, 77-101.

Irvine, T.N., 1965. Chromian spinel as a petrogenetic indicator, Part 1. Theory. Can. J. Earth Sci., 2, 648-672.

Keresztury, G., 2006. Raman Spectroscopy: Theory. In: Handbook of Vibrational Spectroscopy, pp 71-87. https://doi.org/10.1002/0470027320.s0109.

Kharbish, S., 2018. Raman spectroscopic features of Al- Fe^{3+}- poor magnesiochromite and Fe^{2+}- Fe^{3+}- rich ferrian chromite solid solutions. Miner. Petrol., 112, 245-256.

Klein, F. and Garrido, C.J., 2011. Thermodynamic constraints on mineral carbonation of serpentinized peridotite. Lithos, 126, 147-160.

Klein, F., Bach, W. and McCollom, T.M., 2013. Compositional controls on hydrogen generation during serpentinization of ultramafic rocks. Lithos, 178, 55-69.

Kraemer, D., Frei, R., Ernst, D.M., Bau, M. and Melchiorre, E., 2021. Serpentinization in the Archean and Early Phanerozoic – insights from chromium isotope and REY systematics of the Mg–Cr hydroxycarbonate stichtite and associated host serpentinites. Chem. Geol., 565, 120055. https://doi.org/10.1016/j.chemgeo.2020.120055.

Lafuente, B., Downs, R.T., Yang, H. and Stone, N., 2015. The power of databases: the RRUFF project. In: Highlights in Mineralogical Crystallography, T. Armbruster & R.M. Danisi, eds. Berlin, pp 1-30.

Latypov, R., Chistyakova, S. and Mukherjee, R., 2017. A novel hypothesis for origin of massive chromitites in the Bushveld Igneous Complex. J. Petrol., 58(10), 1899-1940.

Latypov, R., Christyakova, S., Barnes, S.J., Godel, B., Delaney, G.W., Cleary, P.W., Radermacher, V.J., Campbell, I. and Jakata, K., 2022. Chromitite layers indicate the existence of large, long-lived, and entirely molten magma chambers. Sci. Rep., 12, 4092. https://doi.org/10.1038/s41598-022-08110-6.

Li, J., Chou, I.M., Wang, X., Liu, Y., Han, Z. and Gao, J., 2025. Pressure sensor based on the Raman shift of the 128 cm^{-1} band of quartz for pressure measurements in hydrothermal diamond-anvil cells. Chem. Geol., 674, 122558. https://doi.org/10.1016/j.chemgeo.2024.122558.

Liu, L., Mernagh, T.P. and Hibberson, W.O., 1997. Raman spectra of high-pressure polymorphs of SiO_2 at various temperatures. Phys. Chem. Miner., 24, 396-402.

Liu, R., Zhao, J., Zhou, M. and Qi, H., 2023. Alteration of chromite during serpentinization of peridotites. Lithos, 460-461, 107385. https://doi.org/10.1016/j.lithos.2023.107385.

Lofgren, G.E., 1983. Effect of heterogeneous nucleation on basaltic textures: a dynamic crystallization study. J. Petrol., 24, 229-255.

Lowell, R.P. and Rona, P.A., 2002. Seafloor hydrothermal systems driven by the serpentinization of peridotite. Geophys. Res. Lett., 29(11), 1531, 261-264. https://doi.org/10.1029/2001GL014411.

Lughi, V., Lenaz, D., Bonifacio, A., Princivalle, F., Sergo, V. and Parisi, F., 2020. A Raman spectroscopy study of the oxidation processes in synthetic chromite $FeCr_2O_4$. Ceram. Int., 46, 29382-29387.

Majumdar, A.S., Hovelmann, J., Mondal, S.K. and Putnis, A., 2016. The role of reacting solution and temperature on compositional evolution during harzburgite alteration: Constraints from the Mesoarchean Nuasahi Massif (eastern India). Lithos, 256-257, 228-242.

McCollom, T.M. and Bach, W., 2009. Thermodynamic constraints on hydrogen generation during serpentinization of ultramafic rocks. Geochim. Cosmochim. Acta, 73, 856-875.

McMillan, P., 1984. Structural studies of silicate glasses and melts – applications and limitations of Raman spectroscopy. Am. Min., 69, 622-644.

McMillan, P.F., 1989. Raman spectroscopy in mineralogy and geochemistry. Ann. Rev. Earth Planet. Sci., 17, 255-283.

Mishra, S. and Gupta, S., 2013. Superposed deformation and inherited structures in an ancient dilational step-over zone: post-mortem of the Rengali Province, India. J. Structural Geol., doi: 10.1016/jsg.2013.11.004.

Moody, J.B., 1976. Serpentinization: a review. Lithos, 9, 125-138.

Murck, B.W. and Campbell, I.H., 1986. The effects of temperature, oxygen fugacity and melt composition on the behaviour of chromium in basic and ultrabasic melts. Geochim. Cosmochim. Acta, 50, 1871-1887.

Nestola, F., Periotto, B., Andreozzi, G.B., Bruschini, E. and Bosi, F., 2014. Pressure-volume equation of state for chromite and magnesiochromite: A single-crystal X-ray diffraction investigation. Am. Min., 99, 1248-1253.

Neuville, D.R., de Ligny, D. and Henderson, G.S., 2014. Advances in Raman spectroscopy applied to earth and material sciences. Rev. Min. Geochem., 78, 509-541.

Oze, C., Fendorf, S., Bird, D.K. and Coleman, R.G., 2004. Chromium geochemistry of serpentine soils. Int. Geol. Rev., 46(2), 97-126.

Pandit, D., 2024. Characterization of Sulphide Ore Minerals Using Combined Laser Raman with Scanning Near-field Optical Microscopy (SNOM). J. Sci. Res., 68(3), 1-5.

Polacci, M., Arzilli, F., La Spina, G., Le Gall, N., Cai, B., Hartley, M.E., Di Geneova, D., Vo, N.T., Nonni, S., Atwood, R.C., Llewellin, E.W., Lee, P.D. and Burton, M.R., 2018. Crystallisation in basaltic magmas revealed via in situ 4D synchrotron X-ray microtomography. Sci. Rep., 8, 8377. https://doi.org/10.1038/s41598-018-26644-6.

Raman, C.V., 1922. Molecular diffraction of light. University of Calcutta, pp 1-103. http://dspace.rri.res.in/handle/2289/2180.

Raman, C.V., 1923. The scattering of light by liquid and solid surfaces. Nature, 112, 281-282. https://doi.org/10.1038/112281a0.

Raman, C.V., 1927. The scattering of light in amorphous solids. J. Opt. Soc. Am., 15(4), 185-189. https://doi.org/10.1364/JOSA.15.000185.

Raman, C.V., 1928. A new radiation. Indian J. Physics, 2, 387-398. http://dspace.rri.res.in/handle/2289/2135.

Raman, C.V., 1929. The Raman effect: investigation of molecular structure by light scattering. Trans. Faraday Soc., 25, 781-792. https://doi.org/10.1039/TF9292500781.

Raman, C.V., 1942. Spectroscopic investigation of the solid and liquid states. Curr. Sci., 11, 225-227. http://dspace.rri.res.in/handle/2289/2199.

Raman, C.V., 1943. The vibration spectrum of a crystal lattice. Proc. Indian Acad. Sci. (Math. Sci.) 18, 237-250. https://doi.org/10.1007/BF03046531.

Raman, C.V., 1945. Scattering of light in crystals. Nature, 155, 396-397. https://doi.org/10.1038/155396a0.

Raman, C.V., 1947. The vibration spectra of crystals. Proc. Indian Acad. Sci., A26, 339-355. https://doi.org/10.1007/BF03170892.

Raman, C.V. and Krishnan, K., 1928. A new type of secondary radiation. Nature, 121, 501-502.

Reddy, B.J. and Frost, R.L., 2005. Spectroscopic characterization of chromite from the Moa-Baracoa Ophiolitic Massif, Cuba. Spectrochim. Acta, Part A 61, 1721-1728.

Rodgers, K.A., 1993. Routine identification of aluminium hydroxide polymorphs with the Laser Raman Microscope. Clay Minerals, 28, 85-99.

Roeder, P.L. and Reynolds, I., 1991. Crystallization of chromite and chromium solubility in basaltic melts. J. Petrol., 32, 909-934.

Saha, A.K., 1994. Crustal evolution of Singhbhum north Orissa, Eastern India. Mem. Geol. Soc. India 27, 1-341.

Sahoo, K.C., 2014. PGE exploration in Odisha: an overview. Indian J. Geosci., 83, 31-37.

Santti, J., Kontinen, A., Sorjonen-Ward, P., Johanson, B. and Pakkanen, L., 2006. Metamorphism and chromite in serpentinized and carbonate-silica-altered peridotites of the Paleoproterozoic Outokumpu-Jormua Ophiolite Belt, eastern Finland. Int. Geol. Rev., 48(6), 494-546.

Schwarzenbach, E.M., Vogel, M., Fruh-Green, G.L. and Boschi, C., 2021. Serpentinization, carbonation, and metasomatism of ultramafic sequences in the Northern Apennine Ophiolite (NW Italy). J. Geophys. Res. Solid Earth, 126, e2020JB020619. https://doi.org/10.1029/2020JB020619.

Shea, T., 2017. Bubble nucleation in magmas: A dominantly heterogeneous process? J. Volcan. Geoth. Res., 343, 155-170. http://dx.doi.org/10.1016/j.jvolgeores.2017.06.025.

Shen, J., Wang, S.J., Qin, L., Ni, H., Li, S., Du, J., Shen, T., Zhang, L. and Yu, H., 2021. Tracing serpentinite dehydration in a subduction channel: chromium element and isotope evidence from subducted oceanic crust. Geochim. Cosmochim. Acta, 313, 1-20. https://doi.org/10.1016/j.gca.2021.06.030.

Singh, A.K. and Pandit, D., 2025. Petrography and Laser Raman Characterization of Banded Hematite Jasper from Agori Formation of Mahakoshal Greenstone Belt. J. Scientific Res., 69, 1-7.

Stowe, C.W., 1994. Compositions and tectonic settings of chromite deposits through time. Econ. Geol., 89, 528-546.

Tait, S.R., Huppert, H.E. and Sparks, R.S.J., 1984. The role of compositional convection in the formation of adcumulate rocks. Lithos, 17, 139-146.

Tegner, C. and Wilson, J.R., 1995. Textures in a poikilitic olivine gabbro cumulate: evidence for supercooling. Min. Petrol., 54, 161-173.

Toramaru, A. and Kichise, T., 2023. A new model of crystallization in magmas: Impact of pre-exponential factor of crystal nucleation rate on cooling rate exponent and log-linear crystal size distribution. J. Geophys. Res. Solid Earth, 128, e2023JB026481. https://doi.org/10.1029/2023JB026481.

Tripathy, A.K., Sahoo, K.C., Abhilash, P.K., Chandhury, T., Kar, R.N., Mohanthy, M. and Das, M., 2014. PGE - bearing Chromite cumulates from boninitic ultramafic parentage in Bhuban ultramafic complex (BUC), Odisha. Indian J. Geosci., 68 (2), 223-236.

Ulmer, G.C., 1974. Alteration of chromite during serpentinization in the Pennsylvania-Maryland district. Am. Min., 59, 1236-1241.

Vandenabeele, P., 2013. Practical Raman Spectroscopy - An Introduction. John Wiley & Sons, Ltd. DOI:10.1002/ 9781119961284.

Wager, L.R., 1959. Differing powers of crystal nucleation as a factor producing diversity in layered igneous intrusions. Geol. Mag., 96, 75-80.

Wager, L.R., Brown, G.M. and Wadsworth, W.J., 1960. Types of igneous cumulates. J. Petrol., 1(1), 73-85.

White, W.B. and Minser, D.G., 1984. Raman spectra and structure of natural glasses. J. Non-Cryst. Solids, 67, 45-59.

Zhang, Z.W. and Gan, F.X., 2011. Analysis of the chromite inclusions found in nephrite minerals obtained from different deposits using SEM-EDS and LRS. J. Raman Spectrosc., 42(9), 1808-1811.

Received on: 7-10-2025; Revised on: 25-1-2026; Accepted on: 30-01-2026